Production of nuclei and hypernuclei in pion-induced reactions near threshold energies

Apiwit Kittiratpattana[1,2] Tom Reichert[1,3] Nihal Buyukcizmeci[4] Alexander Botvina,[1,3] Ayut Limphirat,[2]
Christoph Herold[2,*] Jan Steinheimer,[5] and Marcus Bleicher[1,3]

[1]*Institut für Theoretische Physik, Goethe Universität Frankfurt, Max-von-Laue-Str. 1, D-60438 Frankfurt am Main, Germany*
[2]*Center of Excellence in High Energy Physics and Astrophysics, School of Physics, Suranaree University of Technology,
University Avenue 111, Nakhon Ratchasima 30000, Thailand*
[3]*Helmholtz Research Academy Hesse for FAIR (HFHF), GSI Helmholtzzentrum für Schwerionenforschung GmbH,
Campus Frankfurt, Max-von-Laue-Str. 12, 60438 Frankfurt am Main, Germany*
[4]*Department of Physics, Selcuk University, 42079 Kampüs, Konya, Turkey*
[5]*Frankfurt Institute for Advanced Studies, Ruth-Moufang-Str. 1, D-60438 Frankfurt am Main, Germany*

The ultrarelativistic quantum molecular dynamics model is employed to simulate $\pi^- + $ C and $\pi^- + $ W collisions at $p_{\text{lab}} = 1.7$ GeV motivated by the recent HADES results. By comparing the proton and Λ transverse momentum spectra, it was observed that the data and transport model calculation show a good agreement, if cluster formation is included to obtain the free proton spectra. Predictions of light cluster (d, t, ^{3}He, ^{4}He, as well as $^3_\Lambda$H and ΞN) multiplicities and spectra are made using a coalescence mechanism. The resulting multiplicities suggest that the pion beam experiment can produce a substantial amount of $^3_\Lambda$H, especially in $\pi^- + $ W collisions due to the stopping of the Λ inside the large tungsten nucleus. The findings are supplemented by a statistical multifragmentation analysis suggesting that even larger hyperfragments are produced copiously. It is suggested that even double strange hypernuclei are in reach and might be studied in more detail using a slightly higher pion beam momentum.

I. INTRODUCTION

The production of hypernuclei and nonstrange clusters is currently under study at a large variety of heavy ion accelerator facilities. Heavy ion experiments at the BNL Relativistic Heavy Ion Collider (RHIC) and CERN Large Hadron Collider (LHC) have recently published detailed studies on the production of hypernuclei with a special focus on light hypernuclei, e.g., the hypertriton ($^3_\Lambda$H) [1–8]. It was suggested [9] that the specific structure of the hypertriton, consisting of a deuteron core with a weakly bound Λ, would result in a specific system size dependence of the hypertriton production yield. Generally, however, the data situation for hypernuclei production is rather limited especially for small systems. While at high energies and large systems new experimental data on light hypernuclei and nonstrange cluster production is available, the situation for smaller systems and lower collision energies is different. Here, the HADES experiment [10] can close a gap with its recently measured data using a pion beam with a momentum of 1.7 GeV on a carbon (C) and tungsten (W) target to investigate hypernuclei production in small systems and at low energies.

These reactions are very important, since they are nearby the threshold for hypermatter production. At the same time they produce hyperons with relatively low momenta with

respect to the center-of-mass system. Therefore, investigating the evolution of hypermatter at low energies the study of large hypernuclei becomes possible.

In such a specific collision set up the possible reaction channels are well understood and the environment is rather clean. Generally, the reaction proceeds via the excitation of a baryonic resonance, $\pi^- + n \to \Delta^{*,-}$ or $\pi^- + p \to \Delta^{*,0}$ or N^*, with a typical mass of the Δ or N^* resonance of 2 GeV. The baryon resonance (moving forward with respect to the target system) then decays after approximately 1–2 fm/c mostly into $\pi + N$ (leading to the production of protons and neutrons in the forward direction). However, the resonance may also lead to the production of Λ's via the decay into $\Lambda + K$, and even Ξ production is possible [11]. Further interaction of the Λ or cascade inside the nucleus may slow down the Λ/Ξ and allow for a binding or multifragmentation into a hypernucleus of varying size. The deceleration of the hyperon will of course depend on the size of the target nucleus and is more pronounced in the bigger tungsten than in the carbon target.

The pion beam measurements at HADES [12] therefore open a new route to explore the properties of hypernuclei under rather well controlled and different conditions than at the LHC [13]. This process may further allow to create larger hypernuclei than at the LHC (or even double strange hypernuclei) to explore the properties of strange matter which are relevant for the physics of neutron stars [14–17].

To elucidate some of the questions above and showcase the potential of the pion beam measurements at HADES, we perform the first baseline predictions for the production

*Corresponding author: herold@g.sut.ac.th

of nonstrange and strange clusters in $\pi^- + $ C and $\pi^- + $ W collisions.

To this aim, we will employ a hybrid approach including the dynamical ultrarelativistic quantum molecular dynamics (UrQMD) model, the coalescence, and the statistical multi-fragmentation model for the emitted coalescent clusters which can be in local equilibrium. The latter is a novel development and it avoids the energy balance limitations of the simplistic coalescence and its simple modifications, e.g., via the Wigner function approach. The coalescence model has been previously used to successfully describe the production of nonstrange light nuclei, i.e., deuterons, tritons, and helium and also the strange hypertriton and further strange clusters which have not yet been measured [18–21]. These results are compared to the results of the statistical multifragmentation approach which allows to produce (hyper)nuclei with large mass numbers relative to the system size [22–25].

II. MODEL SETUP

For this study the state-of-the-art UrQMD model (UrQMD v3.5) [26–28] is used. UrQMD is based on the covariant propagation of hadrons (the effective degrees of freedom) and hence provides an effective solution of the relativistic n-particle transport equation. As a QMD-type simulation, all n-particle correlations are kept track of during the system evolution. The imaginary part of the interactions is modeled via binary elastic and inelastic collisions which can excite resonances or color flux tubes which then decay or fragment into hadrons. Potential interactions, modeling the real part of the interactions, can be switched on. For the present study, however, potentials are not employed, instead a coalescence model and the statistical multifragmentation model (SMM) [29] are used to calculate clusters.

A. Coalescence

The production of light clusters and hypernuclei in UrQMD follows the coalescence approach, i.e., light (hyper)nuclei are formed on the kinetic freeze-out hypersurface from their constituents by coalescence. Cluster production via the coalescence mechanism has already proven to reliably describe cluster data over a broad range of collision energies and system sizes with two physics-motivated, energy independent parameters Δx and Δp (or relative velocity Δv). For more details about the specific implementation of coalescence at the kinetic freeze-out and for the specific parameters we refer the reader to [19,30] for light clusters and to [20,21] for hypernuclei.

B. Multifragmentation

Since in $\pi + A$ reactions most of the (hyper)clusters are produced in the region of the nuclear target, we contrasted our simulations using coalescence with calculations employing the multifragmentation approach. Here, one assumes the formation of a larger excited nuclear system, which subsequently fragments into small parts leading to strange [31] and nonstrange clusters as fragmentation products. The SMM is

well tested, the details of the employed approach are described in [22,23,29].

III. RESULTS

All results are obtained by simulating 1.46×10^8 and 4.1×10^7 events of minimum bias $\pi^- + $ C and $\pi^- + $ W collisions[1] with the UrQMD model in version 3.5. All calculations are done in the target rest frame (laboratory frame in the HADES experiment). The rapidity variable y thus refers to the target rest frame, i.e., $y_{target} = 0$. We note that in order to be compared to the experimental data, the free Λ's always include the Σ^0's as the latter ones decay into the Λ and cannot be distinguished in the experiment from initial Λ's. However, the coalescence and multifragmentation routines only consider initial Λ's as the decay of the Σ^0 happens far away due to its comparatively long lifetime. Further Σ^0's do not form hypernuclei (or only barely) and do not contribute to the production of hypertritons. In the present simulation protons do not include feed down from the Λ decay. The units used for $d^2\sigma/dp_T dy$ are μb/(GeVΔy) and for $d\sigma/dy$ it is μb/Δy which are chosen in line with the presented HADES measurements [32]. The coalescence results originating from UrQMD are evaluated at the respective kinetic freeze-out of the particles, while the SMM employs input from the UrQMD at a fixed time which is set to 20 fm/c in the present analysis. Furthermore all particles (including those which are identified as spectators by UrQMD) are given to the statistical multi-fragmentation approach. The coalescence parameter for the primary hot cluster recognition in the SMM model has been set to $v_c = 0.22$ as this value has been shown to provide good results [22,23,33].

A. Transverse momentum spectra of protons and Λ hyperons

We start the investigation by inspecting the double differential transverse momentum spectra of the protons and the Λ's.

Figure 1 shows the transverse momentum differential cross section $d^2\sigma/dp_T dy$ in μb/(GeVΔy) of protons as a function of transverse momentum in different rapidity bins (from $0 \leqslant y < 0.1$ to $0.9 \leqslant y < 1.0$, the curves are successively multiplied by factors of 10 from bottom to top) for minimum bias $\pi^- + $ C (left panel) and $\pi^- + $ W (right panel) collisions from UrQMD (v3.5). The solid lines with symbols show the calculations. The open symbols show the recent HADES measurements [32] and the dotted line shows the exponential curve[2] fitted to the simulation data in the same p_T acceptance

---

[1]We define minimum bias collisions for $\pi^- + $ C with the impact parameter range $0 < b < 2.5$ fm and omit events without any interaction, the total cross section used for the normalization is then $\sigma_{tot}^{\pi^- + C} = 196.35$ mb. For $\pi^- + $ W we use the impact parameter range $0 < b < 6.5$ fm and also omit events without any interaction, the total cross section used for the normalization is then $\sigma_{tot}^{\pi^- + W} = 1327.32$ mb.

[2]Exponential function parametrized by the yield integral and slope parameter $\sim C(y)p_T\sqrt{p_T^2 + m_0^2} \exp[-\sqrt{p_T^2 + m_0^2}/T(y)]$ in line with the HADES analysis [32].
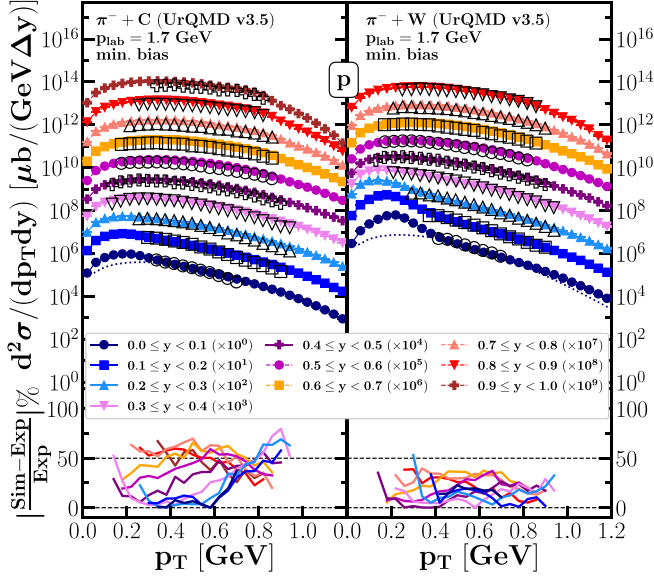
FIG. 1. Upper panel: The transverse momentum differential cross section $d^2\sigma/dp_{\mathrm{T}}dy$ in μb/(GeVΔy) of free protons as a function of transverse momentum in different rapidity bins (from $0 \leqslant y < 0.1$ to $0.9 \leqslant y < 1.0$, the curves are successively multiplied by factors of 10 from bottom to top) for minimum bias $\pi^- + $ C (left) and $\pi^- + $ W (right) collisions from UrQMD (v3.5). The solid lines with symbols show the calculations and the open symbols show the recent HADES measurements [32]. The dotted line shows the extrapolation function used by HADES. Lower panel: The percentage error between the UrQMD simulations and the experimental data.

FIG. 2. Upper panel: The transverse momentum differential cross section $d^2\sigma/dp_{\mathrm{T}}dy$ in μb/(GeVΔy) of Λ as a function of transverse momentum in different rapidity bins (from $0 \leqslant y < 0.15$ to $0.9 \leqslant y < 1.05$, the curves are successively multiplied by factors of 100 from bottom to top) for minimum bias $\pi^- + $ C (left) and $\pi^- + $ W (right) collisions from UrQMD (v3.5). The solid lines with symbols show the calculations and the open symbols show the recent HADES measurements [32]. Lower panel: The percentage error between the UrQMD simulations and the experimental data (the last rapidity bin is scaled by a factor of 0.2 for visibility).

as in the HADES setup. We chose to show the exponential fit of the transverse momentum spectra only in the rapidity window $0 \leqslant y < 0.1$ for brevity in the plot. The percentage error between the UrQMD simulations and the experimental data is shown in the lower panel.

One observes that the UrQMD model calculations of the differential cross section for protons agree qualitatively well with the experimental data [32] in the acceptance region in both collision systems and over all investigated rapidity bins. The slope parameters in the model and the data agree well. A very prominent effect in the proton distributions is noticeable at low rapidity: The UrQMD simulation shows more protons with relatively low transverse momenta and at low rapidity than from the exponential fit to the data, as expected. These are mostly spectator-like nucleons which will eventually form large excited residues decaying into fragments on the later reaction stages. Unfortunately, due to the acceptance of the HADES detector, the phase space region in which the residual nucleus is located (i.e., around zero rapidity and small transverse momenta) is not fully covered by the experiment. Thus, the experiment cannot directly observe the residue free protons at transverse momenta $p_{\mathrm{T}} \leqslant 0.4$ GeV around zero rapidity experimentally. The effect is apparent for both systems and becomes stronger as the system size increases. We will see in the next section that the use of experimental extrapolation results in slightly different rapidity densities near $y \approx 0$.

Figure 2 shows the transverse momentum differential cross section $d^2\sigma/dp_{\mathrm{T}}dy$ in μb/(GeVΔy) of Λ's as a function of

transverse momentum in different rapidity bins (from $0 \leqslant y < 0.15$ to $0.9 \leqslant y < 1.05$, the curves are successively multiplied by factors of 100 from bottom to top) for minimum bias $\pi^- + $ C (left panel) and $\pi^- + $ W (right panel) collisions from UrQMD (v3.5). The solid lines with symbols show the calculations and the open symbols show the recent HADES measurements [32]. The deviation between the UrQMD simulations and experimental data is shown in the lower panel.

The UrQMD model calculations agree well with the data across the transverse momentum range in all rapidity bins with the sharp drop-off behaviors at high p_{T} values. This drop-off in the transverse momentum spectrum towards higher rapidities arises from the limited available energy in the collision.

B. Rapidity distributions of protons and Λ hyperons

Figure 3 shows the rapidity differential cross section $d\sigma/dy$ in μb/Δy of protons (red) and Λ's (orange) as a function of the rapidity for minimum bias $\pi^- + $ C (left panel) and $\pi^- + $ W (right panel) collisions. The results from UrQMD are shown as colored lines with symbols and open black symbols without lines depict the recent HADES measurements [32].

The discussion begins with the rapidity spectra of protons. First the free protons obtained through UrQMD (solid red line with full circles) should be compared to all protons (including those bound in clusters via coalescence, shown as open red circles with dotted lines). One clearly observes that at forward
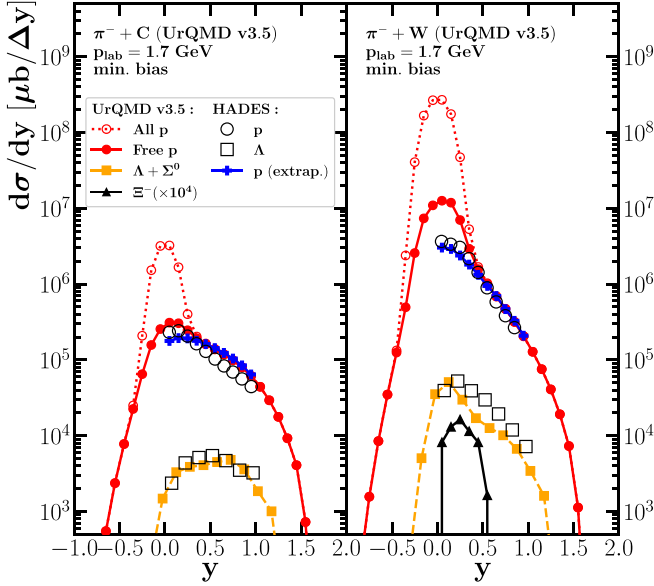
FIG. 3. The rapidity differential cross section $d\sigma/dy$ in μb/Δy of protons (red), Λ's (orange), and Ξ's (black) as a function of the rapidity for minimum bias $\pi^- + $ C (left panel) and $\pi^- + $ W (right panel) collisions. The results from UrQMD are shown as colored lines with symbols, while the open black symbols without lines depict the recent HADES measurements [32]. The blue crosses show the result using the experimental fit function for the p_{T} extrapolation.

FIG. 4. The transverse momentum differential cross section $d^2\sigma/dp_{\mathrm{T}}dy$ in μb/(GeVΔy) of deuterons as a function of transverse momentum in different rapidity bins (from $0 \leqslant y < 0.1$ to $0.8 \leqslant y < 0.9$, the curves are successively multiplied by factors of 100 from bottom to top) for minimum bias $\pi^- + $ C (left panel) and $\pi^- + $ W (right panel) collisions from UrQMD.

and backward rapidities the distributions match each other and describe the HADES data (shown as black open symbols) very well. Only in the target rapidity region the calculated proton spectra differ. The difference is obviously accounted to cluster formation as well as to spectator identification. However, there is a remaining difference between the free protons from the simulation and the data. This difference can be traced back to the extrapolation used in the experiment towards low p_{T} (Sec. III A and Fig. 1). Using the same extrapolation as in the experimental data leads to the blue line with the crosses, which matches the experimental data very well and fully resolves the tension between the calculation and the data in the target region. We therefore suggest that future investigations adjust their fit function to account for these residue free protons.

The measured Λ distribution in the $\pi^- + $ C collision system is well described by the UrQMD model calculations, while in the larger $\pi^- + $ W system, the Λ production in forward direction is slightly underestimated as compared to the experimental data. However, the general trend and multiplicity is captured well providing a reasonable description of the proton and Λ distributions in longitudinal and transverse direction for both collision systems which allows to investigate light and hypercluster production in further detail.

Let us finally note that even in at such low energy also the production of Ξ baryons is possible (black triangles) in the large tungsten system with a cross section on the order of a few μb. This may open the exciting possibility to explore multistrange hyperclusters similar to the approach suggested in [34] although without the need for an antiproton beam.
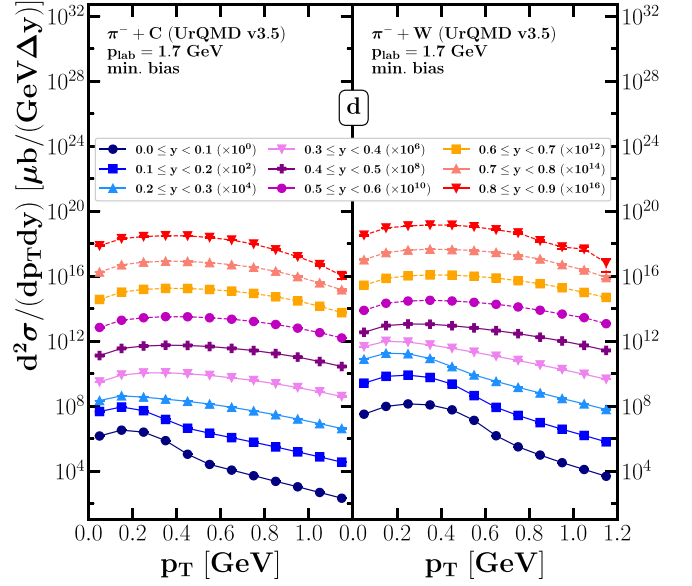
C. Transverse momentum spectra and rapidity distribution of light clusters

After having benchmarked the proton and Λ spectra, we are now ready to address cluster production.

In Fig. 4 the transverse momentum differential cross section $d^2\sigma/dp_{\mathrm{T}}dy$ in μb/(GeVΔy) of deuterons as a function of transverse momentum in different rapidity bins (from $0 \leqslant y < 0.1$ to $0.8 \leqslant y < 0.9$) are shown for minimum bias $\pi^- + $ C (left panel) and $\pi^- + $ W (right panel) collisions from UrQMD. The curves are successively multiplied by factors of 100 from bottom to top for better visibility.

Next, we present in Fig. 5 the transverse momentum differential cross section $d^2\sigma/dp_{\mathrm{T}}dy$ in μb/(GeVΔy) of tritons as a function of transverse momentum in different rapidity bins (from $0 \leqslant y < 0.1$ to $0.5 \leqslant y < 0.6$, the curves are successively multiplied by factors of 100 from bottom to top) for minimum bias $\pi^- + $ C (left panel) and $\pi^- + $ W (right panel) collisions from UrQMD.

Finally, Fig. 6 shows the transverse momentum differential cross section $d^2\sigma/dp_{\mathrm{T}}dy$ in μb/(GeVΔy) of ^{3}He as a function of transverse momentum in different rapidity bins (from $0 \leqslant y < 0.1$ to $0.5 \leqslant y < 0.6$, the curves are successively multiplied by factors of 100 from bottom to top) for minimum bias $\pi^- + $ C (left panel) and $\pi^- + $ W (right panel) collisions from UrQMD.

Generally, we observe a substantial amount of cluster production, especially in the target rapidity region.

We summarize our results in Fig. 7 showing a comparison for the rapidity differential cross section $d\sigma/dy$ in μb/Δy of deuterons (orange), tritons (green), ^{3}He (blue), and ^{4}He (red) as a function of the rapidity for minimum bias $\pi^- + $ C (left
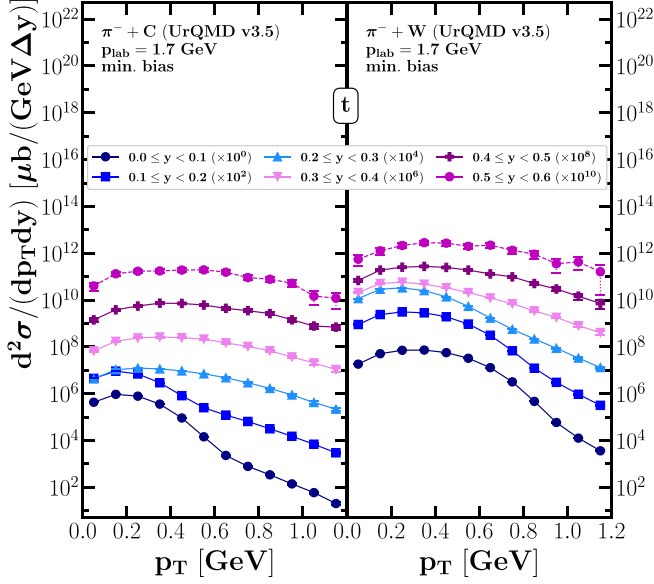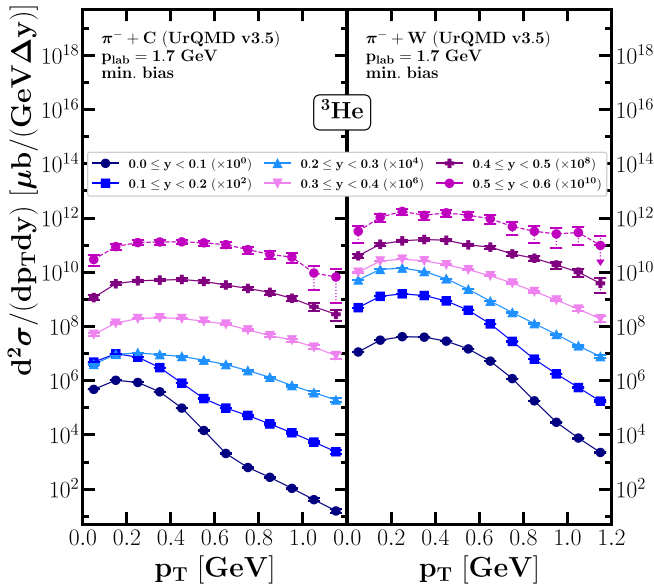
FIG. 5. The transverse momentum differential cross section $d^2\sigma/dp_T dy$ in μb/(GeVΔy) of tritons as a function of transverse momentum in different rapidity bins (from $0 \leqslant y < 0.1$ to $0.5 \leqslant y < 0.6$, the curves are successively multiplied by factors of 100 from bottom to top) for minimum bias $\pi^- + C$ (left panel) and $\pi^- + W$ (right panel) collisions from UrQMD.
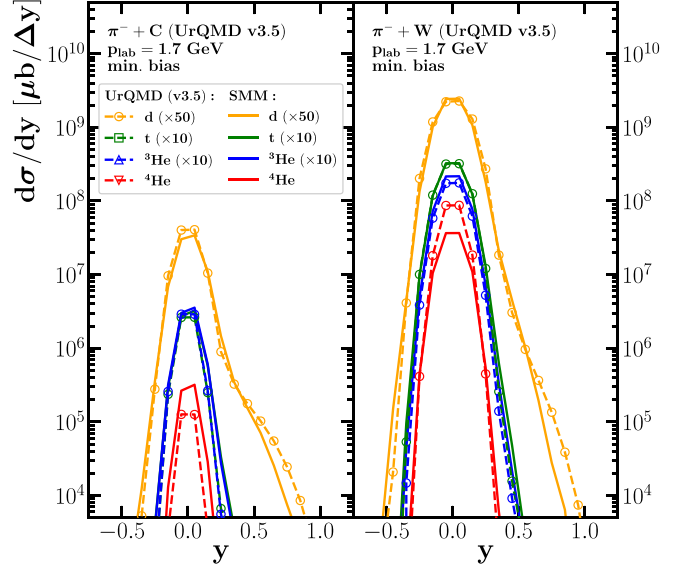
panel) and $\pi^- + W$ (right panel) collisions from UrQMD denoted as dashed lines with open symbols. We further compare yields from the UrQMD coalescence approach to the SMM yields denoted by solid lines without symbols.

FIG. 6. The transverse momentum differential cross section $d^2\sigma/dp_T dy$ in μb/(GeVΔy) of ^{3}He as a function of transverse momentum in different rapidity bins (from $0 \leqslant y < 0.1$ to $0.5 \leqslant y < 0.6$, the curves are successively multiplied by factors of 100 from bottom to top) for minimum bias $\pi^- + C$ (left panel) and $\pi^- + W$ (right panel) collisions from UrQMD.

FIG. 7. The rapidity differential cross section $d\sigma/dy$ in μb/Δy of deuterons (orange), tritons (green), ^{3}He (blue), and ^{4}He (red) as a function of the rapidity for minimum bias $\pi^- + C$ (left panel) and $\pi^- + W$ (right panel) collisions from UrQMD (v3.5) as denoted by dashed lines with symbols and from SMM as denoted by solid lines without symbols.

The peaks of the distributions are centered around target rapidity (i.e., where the residual nucleus is located and fragments). Towards forward rapidity the deuterons show a moderate decrease while the tritons, helium-3, and helium-4 show a rapid decline. This is due to the fact that it is much less likely for the impinging π^- to detach three or more nucleons from the target than two nucleons. We further observe (I) a broadening of the distributions around the peak and (II) a protrusion of the distribution of deuterons and the other investigated nuclei from the peak around the target rapidity in both systems. The physical explanation of (I) is that the broadening is a consequence of the fact that both the coalescence and the multifragmentation processes contribute essentially to the fragment formation around the target region. (II) The protruding part of the deuterons in the carbon system is more discernible than in the tungsten system, indicating a lower stopping power in the smaller carbon system as compared to the tungsten system.

Also, the cluster yields from coalescence (UrQMD) and multifragmentation (SMM) agree very well with each other, which will allow us to use the SMM to extrapolate to high mass hyperclusters.

D. Transverse momentum spectra and rapidity distribution of hypernuclei

Finally, we turn towards the most exciting physics possibilities of the pion beam experiment, namely the production of hypernuclei, and especially the hypertriton. Figure 8 shows the transverse momentum differential cross section $d^2\sigma/dp_T dy$ in μb/(GeVΔy) of the hypertriton $^3_\Lambda$H and the speculated $N\Xi$ clusters as a function of transverse

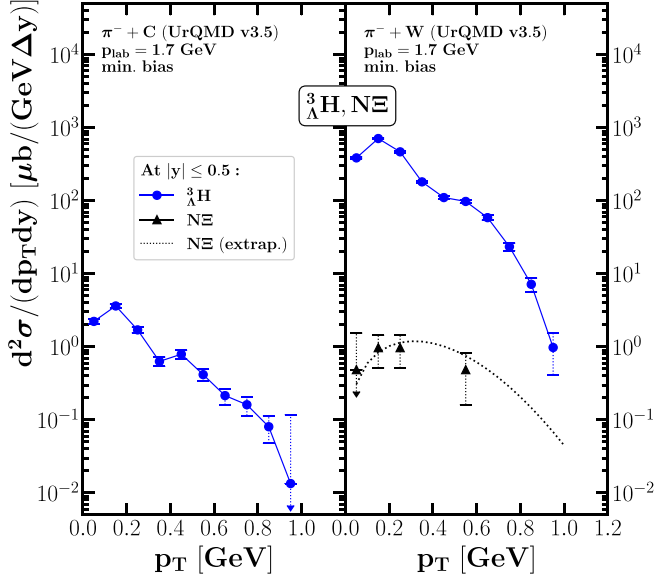FIG. 8. The transverse momentum differential cross section $d^2\sigma/dp_Tdy$ in μb/(GeVΔy) of $^3_\Lambda$H (blue) and $N\Xi$ (black) as a function of transverse momentum at $|y| \leqslant 0.5$, for minimum bias $\pi^- + $ C (left panel) and $\pi^- + $ W (right panel) collisions from UrQMD. The extrapolated $N\Xi$ is shown as a dotted line.

FIG. 9. The rapidity differential cross section $d\sigma/dy$ in μb/Δy of the $N\Lambda$ (blue), $NN\Lambda$ (green), $^3_\Lambda$H (red), $^4_\Lambda$H (yellow), $^4_\Lambda$He (pink), and $N\Xi$ (black) as a function of the rapidity for minimum bias $\pi^- + $ C (left panel) and $\pi^- + $ W (right panel) collisions from UrQMD with coalescence (v3.5) denoted as dashed lines with open symbols and SMM denoted as solid lines with full symbols.

momentum at midrapidity $|y| \leqslant 0.5$ for minimum bias $\pi^- + $ C (left panel) and $\pi^- + $ W (right panel) collisions from UrQMD.

The main observation from the predicted transverse momentum spectra is that the $^3_\Lambda$H is copiously produced with transverse momenta accessible within the HADES acceptance, while $N\Xi$ clusters maybe in reach.

Finally, we combine the different transverse momentum distributions and obtain in Fig. 9 the rapidity differential cross section $d\sigma/dy$ in μb/Δy of the $^3_\Lambda$H (dashed red lines with open symbols), $N\Xi$ (black stars) as well as other clusters as a function of the rapidity for minimum bias $\pi^- + $ C (left panel) and $\pi^- + $ W (right panel) collisions from UrQMD with coalescence denoted by dashed lines and from SMM denoted by solid lines with full symbols.

As expected, the rapidity density of the cross section of $^3_\Lambda$H production has a peak value in the target rapidity region. The yield in the $\pi^- + $ W system is substantially larger than in the $\pi^- + $ C system, due to a higher hyperon multiplicity and due to the larger stopping power of the bigger nucleus, which increases the formation probability. Turning the cross section into numbers, this suggests that $\mathcal{O}(10^{-3})$ hypertritons per event can be expected in these collisions. This means that measured statistics reported by the HADES collaboration (approximately 10^8 recorded events for each system) in Ref. [32] is sufficient to extract up to $\mathcal{O}(10^5)$ $^3_\Lambda$H from their full data set allowing for a detailed and highly differential measurement of the hypertriton.

The light cluster and hypertriton formation from UrQMD and SMM are agreement for the larger system, however for the smaller system they differ by a factor of 10, which may indicate the systematic error for the hypertriton production.
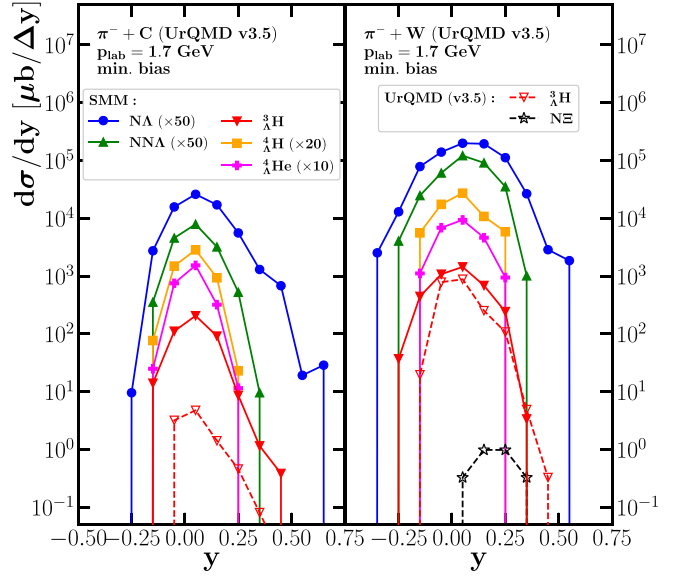
Figure 9 therefore additionally shows the rapidity densities of the $N\Lambda$ (blue line with circles), the $NN\Lambda$ (green line with triangles-up), the $^4_\Lambda$H (yellow line with squares), and the $^4_\Lambda$He (pink line with crosses) as calculated with the SMM model. One observes that these hypernuclei are also produced copiously and confirms that the stopping power from the target nucleus allows only a few nucleons to fly in the forward rapidity direction. As a result, the $N\Lambda$ (blue) formation with $A = 2$ extends more toward forward rapidity compare to other hypernuclei with $A \geqslant 3$.

E. Light and hyperfragments of larger mass numbers

Within the statistical multifragmentation model also larger light nuclei and hypernuclei are formed due to the statistical decay of the residues and excited coalescent clusters. This allows to estimate the total abundance of Λ hypernuclei in the analyzed $\pi^- + $ C/W systems at 1.7 GeV incident momentum.

Figure 10 shows the integrated cross section of light nuclei (full symbols) and hypernuclei (single-strange as open symbols) production with different charges Z (denoted by the color) as a function of their mass number A for minimum bias $\pi^- + $ C and $\pi^- + $ W collisions from a SMM analysis of the UrQMD (v3.5) data. Although the light cluster and hypernuclei abundances fall off approximately exponentially with increasing mass number, a phenomenon also observed in the production of light nuclei at RHIC [35], their integrated production cross section might still allow for a signal extraction by the HADES collaboration or in an upcoming $\pi + A$ experiment with higher beam luminosity. As light nuclear fragments with a mass numbers up to $A = 16$ are still produced with a yield of 10^{-6} per event and hypernuclei with
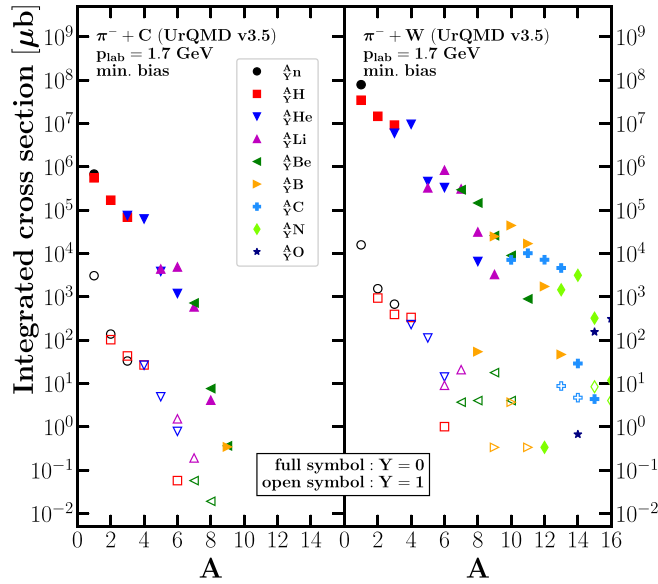
FIG. 10. The integrated cross section of light nuclei (full symbols) and hypernuclei (single-strange as open symbols) production with different charges Z (denoted by the color) as a function of their mass number A for minimum bias $\pi^- + \mathrm{C}$ and $\pi^- + \mathrm{W}$ collisions from a SMM analysis of the UrQMD (v3.5) data.

mass number $A = 10$ with a yield of 10^{-7} per event, this allows for the first time to study light clusters and hypernuclei with large A in πA collisions. As reported by the HADES collaboration in [36] their pion beam can reach beam momenta of up to $p_{\mathrm{beam}} = 2.5$ GeV lifting the abundances drastically and allowing for significant Ξ-hypernuclei production as well. This may offer the unique opportunity to implement parts of the hypermatter physics program proposed for PANDA in the HADES $\pi + A$ program.

IV. CONCLUSION

In this paper we have employed the state-of-the-art UrQMD microscopic transport model to calculate $\pi^- + \mathrm{C}$ and $\pi^- + \mathrm{W}$ collisions at $p_{\mathrm{lab}} = 1.7$ GeV. We found good

agreement between the calculated and measured transverse momentum and rapidity distributions of protons and Λ's. An important aspect for the description of the proton spectra in the target region was the inclusion of cluster production to obtain the free proton spectra using the coalescence approach. We have further contrasted our results on light nuclei and hypernuclei production from a coalescence approach with a SMM. We have predicted the light cluster (deuteron, triton, and helium-3) double differential cross sections and rapidity densities using the coalescence mechanism and SMM model. Finally, we applied the coalescence mechanism and the SMM to predict hypernuclei double differential cross sections. Both nonstrange and strange cluster yields are sufficiently high to be accessible by the HADES collaboration's statistics.

As a final remark, the potential of double strange hypernuclei production is discussed. It was suggested that Ξ production proceeds also via the formation of a resonance that decays via $N^* \to \Xi + K + K$ [37]. If such a resonance exists, then the HADES pion beam set up with a selection of pions with higher momenta (reaching at least a center-of-mass energy of $\sqrt{s} = m_\Xi + 2m_K$) would allow to perform similar studies as with the PANDA detector for multistrange hyperfragments. In the same manner, the double-Λ hypernuclei can be produced via $\Xi + N + N \leftrightarrow \Lambda + \Lambda + N$.

[1] B. I. Abelev *et al.* (STAR Collaboration), Science **328**, 58 (2010).

[2] C. Rappold, E. Kim, D. Nakajima, T. R. Saito, O. Bertini, S. Bianchin, V. Bozkurt, M. Kavatsyuk, Y. Ma, F. Maas *et al.*, Nucl. Phys. A **913**, 170 (2013).

[3] C. Rappold, T. R. Saito, O. Bertini, S. Bianchin, V. Bozkurt, M. Kavatsyuk, E. Kim, Y. Ma, F. Maas, S. Minami *et al.*, Phys. Lett. B **728**, 543 (2014).

[4] J. Adam *et al.* (ALICE Collaboration), Phys. Lett. B **754**, 360 (2016).

[5] L. Adamczyk *et al.* (STAR Collaboration), Phys. Rev. C **97**, 054909 (2018).

[6] J. Adam *et al.* (STAR Collaboration), Nat. Phys. **16**, 409 (2020).

[7] S. Acharya *et al.* (ALICE Collaboration), Phys. Lett. B **797**, 134905 (2019).

[8] M. Abdallah *et al.* (STAR Collaboration), Phys. Rev. Lett. **128**, 202301 (2022).

[9] K. J. Sun, C. M. Ko, and B. Dönigus, Phys. Lett. B **792**, 132 (2019).

[10] G. Agakichiev *et al.* (HADES Collaboration), Eur. Phys. J. A **41**, 243 (2009).

[11] J. Steinheimer, A. Botvina, and M. Bleicher, Phys. Rev. C **95**, 014911 (2017).

[12] J. Adamczewski-Musch *et al.* (HADES Collaboration), Eur. Phys. J. A **53**, 188 (2017).

[13] B. Dönigus, Eur. Phys. J. A **56**, 280 (2020).

[14] F. Özel, D. Psaltis, S. Ransom, P. Demorest, and M. Alford, Astrophys. J. Lett. **724**, L199 (2010).

[15] L. Bonanno and A. Sedrakian, Astron. Astrophys. **539**, A16 (2012).

[16] R. Łastowiecki, D. Blaschke, H. Grigorian, and S. Typel, Acta Phys. Pol. B Proc. Suppl. **5**, 535 (2012).

[17] D. Blaschke and D. E. Alvarez-Castillo, AIP Conf. Proc. **1701**, 020013 (2016).

[18] V. Gaebel, M. Bonne, T. Reichert, A. Burnic, P. Hillmann, and M. Bleicher, Eur. Phys. J. A **57**, 55 (2021).

[19] P. Hillmann, K. Käfer, J. Steinheimer, V. Vovchenko, and M. Bleicher, J. Phys. G **49**, 055107 (2022).

[20] T. Reichert, J. Steinheimer, V. Vovchenko, B. Dönigus, and M. Bleicher, Phys. Rev. C **107**, 014912 (2023).

[21] T. Reichert, J. Steinheimer, V. Vovchenko, B. Dönigus, and M. Bleicher, EPJ Web Conf. **276**, 04008 (2023).

[22] A. S. Botvina, N. Buyukcizmeci, and M. Bleicher, Phys. Rev. C **103**, 064602 (2021).

[23] N. Buyukcizmeci, A. S. Botvina, R. Ogul, and M. Bleicher, Eur. Phys. J. A **56**, 210 (2020).

[24] A. S. Botvina, N. Buyukcizmeci, and M. Bleicher, Phys. Rev. C **106**, 014607 (2022).

[25] N. Buyukcizmeci, T. Reichert, A. S. Botvina, and M. Bleicher, Phys. Rev. C **108**, 054904 (2023).

[26] S. A. Bass, M. Belkacem, M. Bleicher, M. Brandstetter, L. Bravina, C. Ernst, L. Gerland, M. Hofmann, S. Hofmann, J. Konopka *et al.*, Prog. Part. Nucl. Phys. **41**, 255 (1998).

[27] M. Bleicher, E. Zabrodin, C. Spieles, S. A. Bass, C. Ernst, S. Soff, L. Bravina, M. Belkacem, H. Weber, H. Stoecker *et al.*, J. Phys. G **25**, 1859 (1999).

[28] M. Bleicher and E. Bratkovskaya, Prog. Part. Nucl. Phys. **122**, 103920 (2022).

[29] J. P. Bondorf, A. S. Botvina, A. S. Ilinov, I. N. Mishustin, and K. Sneppen, Phys. Rep. **257**, 133 (1995).

[30] S. Sombun, K. Tomuang, A. Limphirat, P. Hillmann, C. Herold, J. Steinheimer, Y. Yan, and M. Bleicher, Phys. Rev. C **99**, 014901 (2019).

[31] A. S. Botvina and J. Pochodzalla, Phys. Rev. C **76**, 024909 (2007).

[32] R. A. Yassine *et al.* (HADES Collaboration), arXiv:2301.03940.

[33] A. S. Botvina, J. Steinheimer, E. Bratkovskaya, M. Bleicher, and J. Pochodzalla, Phys. Lett. B **742**, 7 (2015).

[34] J. Pochodzalla, Acta Phys. Pol. B **42**, 833 (2011).

[35] H. Agakishiev *et al.* (STAR Collaboration), Nature (London) **473**, 353 (2011); **475**, 412(E) (2011).

[36] M. Ardid *et al.* (Pion Collaboration), AIP Conf. Proc. **495**, 401 (1999).

[37] J. Steinheimer and M. Bleicher, J. Phys. G **43**, 015104 (2016).

Correction: The "Corresponding author" indicator and the byline footnote were missing and have been inserted.